ELSEVIER

Journal of Alloys and Compounds 465 (2008) 210–215

Journal of ALLOYS AND COMPOUNDS

www.elsevier.com/locate/jallcom

Low-frequency damping properties of dual-phase Mg–*x*Li–0.5Zn alloys

S.K. Wu [a,*], S.H. Chang [b], T.Y. Chou [a], S. Tong [c]

[a] *Department of Materials Science and Engineering, National Taiwan University, Taipei 106, Taiwan*
[b] *Department of Chemical and Materials Engineering, National I-Lan University, I-Lan 260, Taiwan*
[c] *Chung-shan Institute of Science and Technology, P.O. Box 90008-8-5, Lung-Tan, Taoyuan 325, Taiwan*

Received 22 September 2007; received in revised form 30 October 2007; accepted 30 October 2007
Available online 6 November 2007

Abstract

Low-frequency damping capacities of dual-phase Mg–*x*Li–0.5Zn alloys with $x = 6.0$ (α-rich LZ60), 9.5 (LZ100) and 10.5 (β-rich LZ110) are studied by dynamic mechanical analyzer. Both LZ100 and LZ110 have a significant P_1 peak but only LZ110 exhibits a significant P_2 peak. LZ60 does not show any obvious internal friction peak and has the lowest tan δ value of high-temperature damping background (HTDB). Both P_1 peak and HTDB of LZ100 are frequency dependent and thermal activated with their activation energy being 0.87 and 0.59 eV, respectively. The relatively low activation energy of HTDB for LZ100 is corresponding to the smaller atomic radius of Li atoms in Mg alloys which facilitates the dislocation climbing process at moderately high temperature. The strain amplitude dependence of tan δ value shows that, for LZ100 at room temperature, the critical strain is 3×10^{-5}.

Keywords: Damping; Magnesium–lithium alloys; Dynamic mechanical analyzer; High-temperature damping background

1. Introduction

Magnesium with a density of 1.74 g/cm^3 is the lightest of all structural metals and this characteristic is regarded as the most important factor in the selection and use for engineering designs. Meanwhile, magnesium and magnesium alloys possess high damping capacity due to their good ability to absorb energy elastically [1]. Damping capacities of magnesium and magnesium alloys are reported to be dependent on the strain amplitude, and are considered to be related to the dislocation movement in which the dislocations are weakly pinned by impurity atoms on the basal planes [2]. Since magnesium has the hexagonal close-packed crystal structure, the cold-working amount of magnesium alloys is restricted. Therefore, most magnesium alloys are deformed at elevated temperature by warm/hot working. Lithium is another light-weight metal having a density of only 0.53 g/cm^3. When lithium is added to magnesium, the density of the alloy is reduced and its processability, ductility and superplasticity at relatively low stresses are also improved [3–6]. The Mg–Li binary phase diagram shows that, with Li content between about 5 and 11 wt.%, BCC-structured β phase of Li solid solution will co-exist with HCP-structured α phase of Mg solid solution [7]. α + β dual-phase Mg–Li alloys have been reported to have high elongation with low strength, such as Mg–8.5 wt.% Li and Mg–9 wt.% Li having the elongation of 610% and 460%, respectively, at room temperature [4,8]. Therefore, zinc [9–12], aluminum [12–14] and so on are usually added to strengthen Mg–Li alloys. In this study, α + β dual-phase Mg–*x*Li–0.5Zn alloys with $x = 6.0$, 9.5 and 10.5 wt.% were prepared. The aim of the present work is to study the low-frequency damping capacities of α + β dual-phase Mi–Li alloys with different α and β volumes through strain amplitude and frequency damping tests. According to the experimental results, the characteristics of their damping properties are discussed.

2. Experimental procedures

The alloys used in this study are Mg–*x*Li–0.5Zn (in wt.%) with $x = 6.0$ (LZ60), 9.5 (LZ100) and 10.5 (LZ110). The alloys were processed in a high-frequency induction furnace equipped with vacuum capability and Ar gas used during the cast. The chemical compositions of cast ingots were analyzed by the induction couple plasma (ICP) apparatus. The ingots were rolled at room

* Corresponding author. Tel.: +886 2 2363 7846; fax: +886 2 2363 4562.
E-mail address: skw@ntu.edu.tw (S.K. Wu).

0925-8388/$ – see front matter © 2007 Elsevier B.V. All rights reserved.
doi:10.1016/j.jallcom.2007.10.134

temperature with rollers maintained at 160 °C. The initial 37 mm-thick ingots were thinned down to final 1 mm plates with each pass of rolling undergoing ≈5% thickness reduction. The rolled plates were annealed at 250 °C for 1.5 h and they were the as-annealed plates used in this study. The specimens for dynamic mechanical analyzer (DMA) tests were cut from the as-annealed plates with the specimen's size being 35 mm long and 5 mm wide and their longitudinal direction being along the rolling one. Internal friction tan δ values of as-annealed Mg–*x*Li–0.5Zn specimens were measured by a TA 2980 DMA equipment with a single cantilever at a constant heating rate of 5 °C/min. The testing temperature, frequency and amplitude are used in the range of 0–200 °C, 0.5–50 Hz and 5–20 μm, respectively. The crystallographic features of the as-annealed Mg–*x*Li–0.5Zn alloys were determined using a Philips PW 1830 XRD instrument with Cu Kα radiation. The specimens of as-annealed Mg–*x*Li–0.5Zn alloys for the microstructural observation were prepared by the standard metallographic procedure with the etching solution 35 ml alcohol + 5 ml H_2O + 5 ml picric acid + 5 ml acetic acid and the etching time 5 s.

3. Results and discussion

3.1. Microstructure observations

Fig. 1(a)–(c) shows the as-annealed microstructures of LZ60, LZ100 and LZ110 alloys, respectively, which are observed by a Nikon AFX-DX optical microscopy. As can be seen, the white area is the β phase and the gray one is the α phase. The area percentages occupied by α and β phases are measured by a software "Micrometrics SE (Version 2.6)" for image analysis and the results are 93.6% α, 6.4% β for LZ60 alloy; 57.2% α, 42.8% β for LZ100 alloy and 18.6% α, 81.4% β for LZ110 alloy. Obviously, alloy LZ60 is rich in α phase, LZ110 is rich in β phase and LZ100 has about half–half in α and β phases. Fig. 2 shows the XRD results of the as-annealed Mg–*x*Li–0.5Zn alloys of Fig. 1. In Fig. 2, only diffraction peaks of α and β phases can be observed and those of more intensive peaks are indexed their diffracted planes. The results of Fig. 2 also indicate that LZ60 and LZ110 alloys are primarily composed of α and β phases, respectively.

3.2. Damping characterization of MgLi alloys

Fig. 3 shows the heating tan δ curve versus temperature for as-annealed Mg–*x*Li–0.5Zn alloys with $x = 6.0$, 9.5 and 10.5 wt.%. The DMA experimental parameters used in Fig. 3 are 1 Hz frequency, 20 μm amplitude and 5 °C/min heating rate from 0 to 200 °C. The inset shown in Fig. 3 is the magnified curves in the range of 0–80 °C. As indicated in Fig. 3, the tan δ curve of LZ110 alloy has two internal friction peaks at about 35 °C (termed P_1) and 120 °C (termed P_2), respectively. Both P_1 and P_2 peaks shown in Fig. 3 are also observed in pure Mg with 99.96 wt.% purity and Mg–Ni alloys with 6.2–22.6 wt.% Ni [15]. According to the reported study [15], P_1 peak results from the movement of dislocations on the basal planes and P_2 peak is caused by the sliding of grain boundaries. Except P_1 and P_2 peaks shown in Fig. 3, the heating tan δ curve of LZ110 can be divided into an athermal internal friction background (for temperature below 70 °C) and an exponential internal friction background (for temperature above 70 °C). The exponential internal friction background is also termed as high-temperature damping background (HTDB) which has been observed in many other intermetallics [16–18].

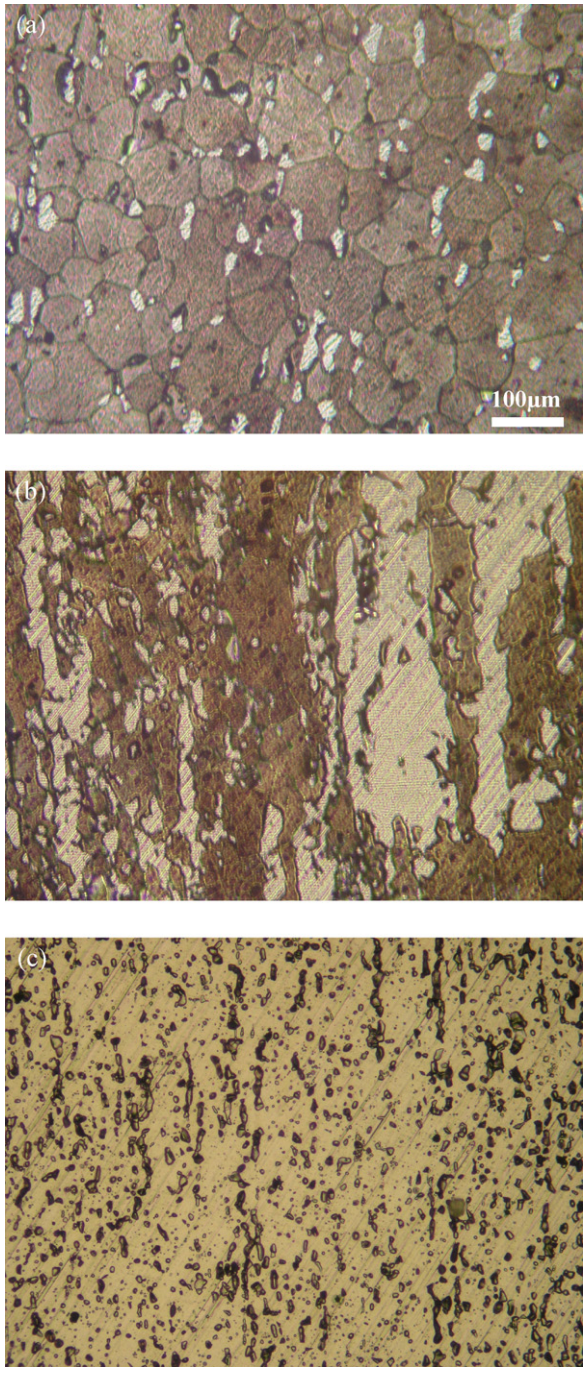

Fig. 1. Microstructural images of as-annealed (a) LZ60 alloy, (b) LZ100 alloy and (c) LZ110 alloy observed by an optical microscopy.

Fig. 3 also illustrates that LZ100 alloy exhibits a well-defined P_1 peak at about 35 °C but no obvious P_2 peak can be found. Meanwhile, the HTDB of LZ100 has a higher tan δ value of HTDB than that of LZ110 when temperature is above 140 °C. However, as shown in Fig. 3, both P_1 and P_2 peaks for LZ60 alloy are insignificant. Besides, LZ60 has the lowest tan δ value in both athermal internal friction background and HTDB among these three alloys. Above results indicate that the microstructure of as-annealed Mg–*x*Li–0.5Zn alloys can significantly influence the damping behavior of internal friction peaks and internal friction

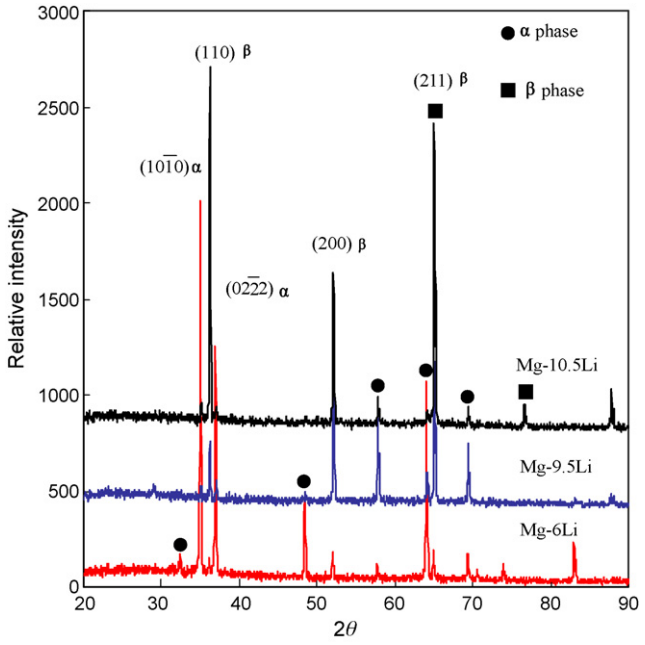

Fig. 2. XRD results of as-annealed LZ60, LZ100 and LZ110 alloys at room temperature.

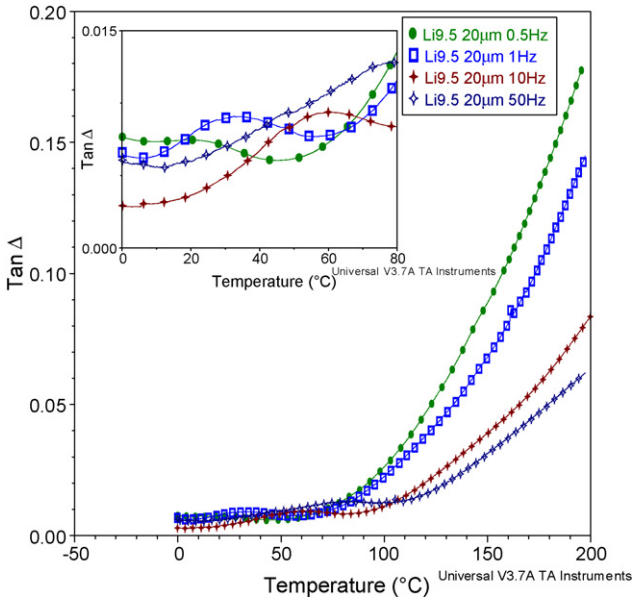

Fig. 4. The tan δ values vs. temperature under various frequencies (0.5–50 Hz) for as-annealed LZ100 alloy. The inset shows the magnified curves in the range of 0–80 °C.

background. Since LZ60 alloy has the lowest tan δ value in both athermal internal friction background and HTDB, it implies that the damping capacity of HCP-structured α phase is inferior to that of BCC-structured β phase. This characteristic is possibly related to the insignificant P_1 and P_2 peaks in LZ60 alloy. Fig. 3 also shows that LZ100 alloy has rather good tan δ values in the overall range of 0–200 °C. Thus, LZ100 alloy is chosen to study its damping capacity as a function of frequency and amplitude, as demonstrated in the following.

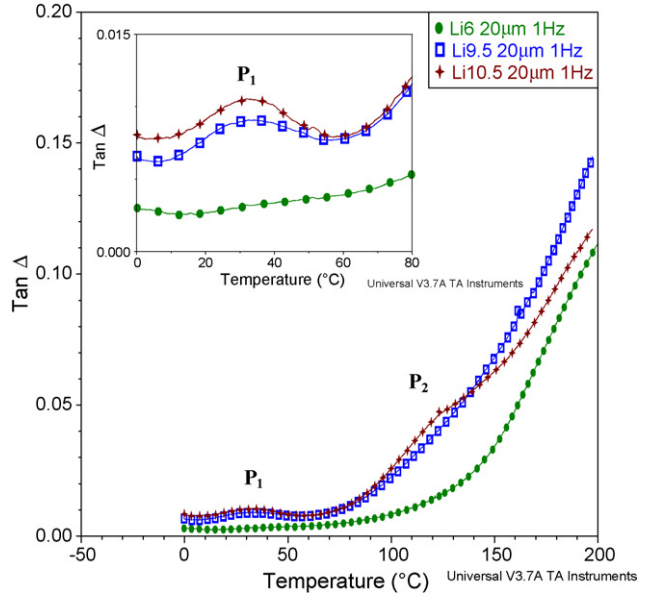

Fig. 3. The tan δ values vs. temperature for as-annealed LZ60, LZ100 and LZ110 alloys measured by DMA. The inset shows the magnified curves in the range of 0–80 °C.

3.3. Frequency and amplitude dependence of LZ100 alloy

Fig. 4 shows the effect of frequency (0.5–50 Hz) on the tan δ value of LZ100 alloy using 5 °C/min heating rate and 20 μm amplitude (strain $\varepsilon = 1.2 \times 10^{-4}$). The inset shown in Fig. 4 is the magnified curves in the range of 0–80 °C. As can be seen, the peak temperature of P_1 shifts to a higher temperature with increasing frequency. This feature indicates that P_1 peak is a thermal activated relaxation process. Meanwhile, the tan δ value of HTDB for LZ100 alloy increases with decreasing frequency at the same temperature. This phenomenon implies that the HTDB of LZ100 alloy exhibits a viscoelastic characteristic at higher temperature. Further discussions on the frequency-dependent characteristics of P_1 peak and HTDB are demonstrated in next section.

Fig. 5 shows the effect of amplitude on damping capacity of LZ100 alloy with the amplitude at 5, 10 and 20 μm and the frequency at 1 Hz. The inset shown in Fig. 5 is the magnified curves in the range of 0–80 °C. The P_1 peak appears at 35 °C with 20 μm amplitude having the highest tan δ value. As shown in Fig. 5, the effect of amplitude on the tan δ value is not so significant except that the temperature is around 150 °C. Fig. 6 shows the dependence of tan δ value on strain amplitude (ε) in LZ100 alloy at room temperature. As can be seen, in the strains lower than 3×10^{-5}, the tan δ value is almost kept constant and is independent or weakly dependent on the strain amplitude. However, in the strains amplitude higher than 3×10^{-5}, the tan δ values increase rapidly with increasing strain amplitude, and finally reach a saturated value at $\varepsilon = 10 \times 10^{-4}$. The critical strain ε_c, which is defined as the transition strain from the strain amplitude independent region to the dependent region, is 3×10^{-5} in Fig. 6. This ε_c value is comparable to that reported in pure Mg of 99.96 wt.% purity, which is 2×10^{-5} [15].

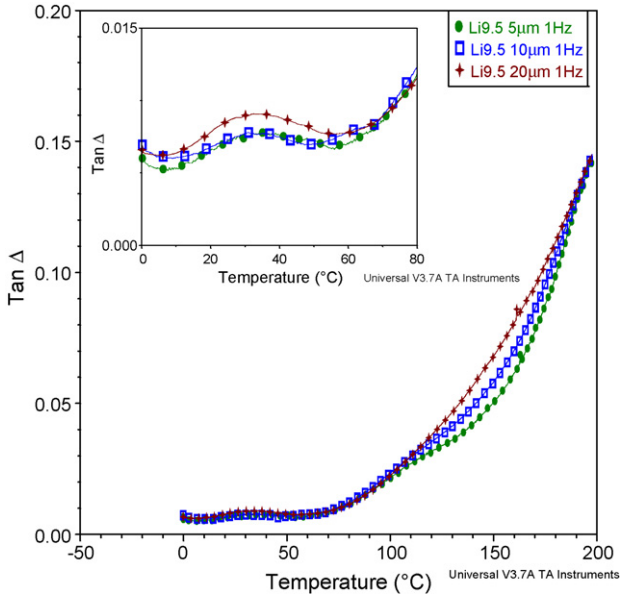

Fig. 5. The tan δ values vs. temperature under various amplitudes (5–20 μm) for as-annealed LZ100 alloy. The inset shows the magnified curves in the range of 0–80 °C.

3.4. Frequency effect on P_1 peak and HTDB of LZ100 alloy

As shown in Fig. 4, the peak temperature of P_1 shifts to a higher temperature when the frequency is increased. This indicates that P_1 peak of LZ100 alloy exhibits a thermal activated relaxation characteristic. Therefore, the relaxation time and activation energy of P_1 peak should follow the Arrhenius equation

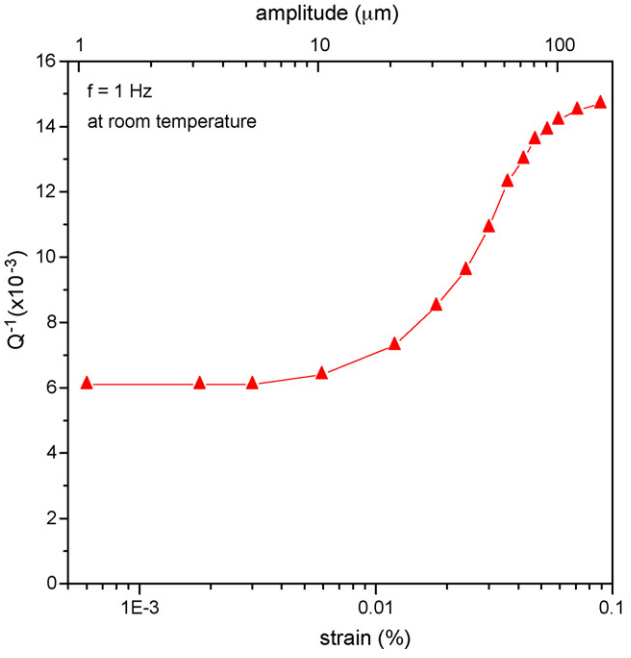

Fig. 6. Strain amplitude dependence of the tan δ values of as-annealed LZ100 alloy at room temperature with 1 Hz frequency. The critical strain ε_c is 3×10^{-5}.

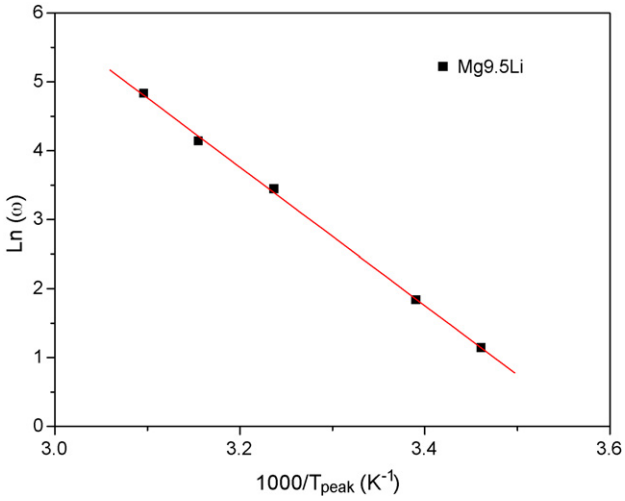

Fig. 7. Arrhenius plot ($\ln \omega$ vs. $1/T$) measured from P_1 peak temperature in Fig. 4.

[19]:

$$\tau = \tau_0 \exp\left(\frac{H}{kT}\right) \quad (1)$$

where τ and τ_0 are the relaxation time and relaxation constant, respectively, H is the activation energy of the dislocation movement, k is the Boltzmann constant and T is the temperature. At peak temperature, relaxation time τ and angle frequency ω satisfy the relationship of $\tau_P \omega_P = 1$. Therefore, Eq. (1) can be rewritten as

$$\omega_P^{-1} = \tau_0 \exp\left(\frac{H}{kT_P}\right) \quad (2)$$

Since τ_P is a function of frequency, the Arrhenius relation of $\ln(\omega)$ versus $1000/T_P$ can be plotted, as shown in Fig. 7, and the activation energy (H) of P_1 peak can be calculated as 0.87 eV. The activation energy of P_1 peak for other magnesium alloys has not been reported yet, however, this low activation energy (0.87 eV) is close to that for the dragging process between dislocations and mobile point-defects in aluminum (about 0.8 eV) [20,21].

Meanwhile, also from Fig. 4, the tan δ value of HTDB for LZ100 alloy increases with decreasing frequency at the same temperature. This feature indicates that the HTDB for LZ100 alloy also exhibits a viscoelastic characteristic. In dynamic experiments, the internal friction can be described as [17]:

$$Q^{-1} \equiv \tan\delta = \frac{1}{\omega\tau} \quad (3)$$

Usually, there exists a distribution of relaxation time which can be taken into account empirically by a spectrum parameter n in Eq. (3) [22]:

$$Q^{-1} = \frac{1}{(\omega\tau)^n} \quad (4)$$

where $0 \le n \le 1$ ($n = 1$ for "ideal" viscoelasticity). Since viscoelastic behavior at high temperature can be determined by a thermally activated process, an Arrhenius equation (Eq. (1))

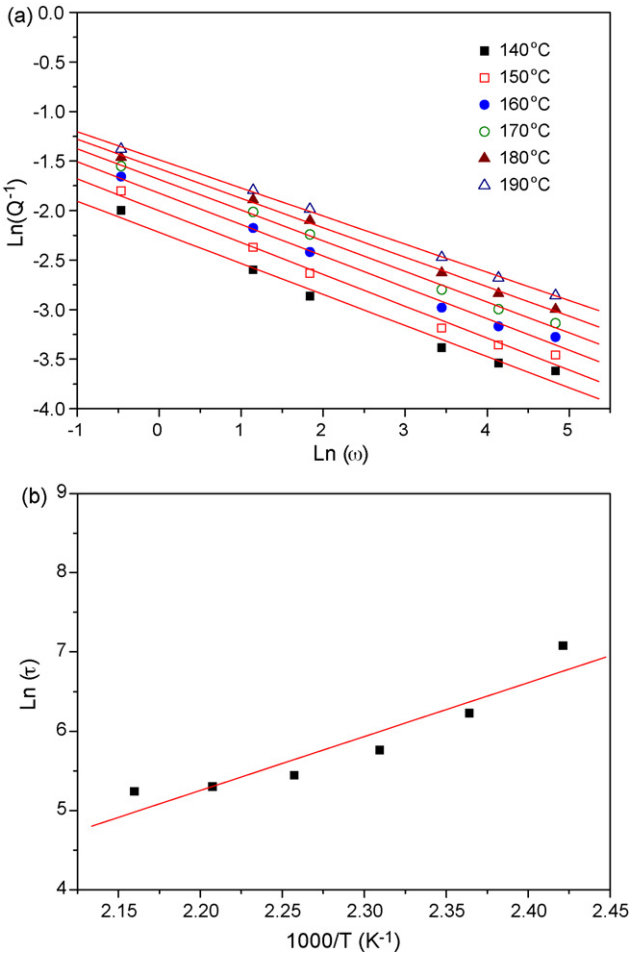

Fig. 8. (a) The plot of $\ln Q^{-1}$ vs. $\ln \omega$ for various temperatures measured from Fig. 4. (b) Arrhenius plot ($\ln \tau$ vs. $1/T$) determined from (a) for LZ100 alloy.

holds for the relaxation time τ. For the analysis of the HTDB, it is convenient to use the logarithmic representation of Eq. (4):

$$\ln Q^{-1}(T, \omega) = -n \ln \omega - n \ln \tau(T) \quad (5)$$

Fig. 8(a) shows the logarithmic plot ($\ln Q^{-1}$ versus $\ln \omega$ for various temperatures) of the HTDB data which are determined at different temperatures above 140 °C in Fig. 4. As shown in Fig. 8(a), the measured $\ln Q^{-1}$ and $\ln \omega$ has a linear dependence which is in accordance with the expectation of the viscoelastic relaxation behavior. From the slope and intercept of the fitting lines shown in Fig. 8(a), the n value and relaxation time (τ) measured at each temperature can be determined. Fig. 8(b) plots the relaxation time (τ) as a function of temperature in which τ is measured from various temperatures in Fig. 8(a). From Fig. 8(b), the activation energy of the HTDB for as-annealed LZ100 alloy can be determined from the slope of the fitting line as the value of $H = 0.59$ eV.

The activation energy of HTDB for Mg alloys has not been investigated in detail before. Nevertheless, in this study, the calculated activation energy of HTDB for annealed LZ100 alloy is much lower than those of reported Al or TiAl alloys, such as Al–4 at.% Mg alloy (about $H = 1.25$ eV) [23], Ti–46 at.% Al–9 at.% Nb alloy (about $H = 4.2$–4.3 eV), Ti–46.5 at.% Al–4 at.% (Cr, Nb, Ta, B) alloy (about $H = 3.8$–3.9 eV) and $Ni_{49.5}Al_{50.5}$ single crystal (about $H = 3.3$ eV) [18]. Besides, LZ100 alloy also exhibits HTDB at a lower temperature than those of Al or TiAl alloys. Weller et al. [18] reported that the HTDB in TiAl and NiAl alloys can be assigned to the diffusion-assisted climb of dislocations since the activation energies of TiAl alloys detected from high-temperature damping experiments and from creep experiments are very similar. Therefore, the lower activation energy of HTDB for annealed LZ100 alloy indicates that the diffusion-assisted dislocations climbing process is easier in LZ100 alloy. At the same time, the calculated activation energy of HTDB for LZ100 is also lower than that of the self-diffusion in pure Mg, say 1.38 eV [24,25], and that of the grain boundary diffusion in pure Mg, say 0.95 eV [26]. This indicates that the addition of Li atoms into Mg matrix can accelerate the solute atoms diffusion process or the grain boundary diffusion process and simultaneously facilitates the dislocation climbing process at moderately high temperature. This characteristic comes from the fact that the smaller atomic radius of Li atom can diffuse more rapidly in the relatively loose BCC-structured β phase and at the abundant α/β phase boundaries in LZ100 alloy.

4. Conclusions

Low-frequency damping capacities of dual-phase Mg–xLi–0.5Zn (in wt.%) with $x = 6.0$ (LZ60), 9.5 (LZ100) and 10.5 (LZ110) are studied by DMA. Microstructural observations and XRD results indicate that LZ60 and LZ110 alloys are rich in α and β phases, respectively, and LZ100 alloy has about half–half in α and β phases. Both LZ100 and LZ110 have a significant P_1 peak but only LZ110 exhibits a significant P_2 peak. LZ60 alloy does not show significant P_1 and P_2 peaks and has the lowest $\tan \delta$ value of HTDB among these three alloys. These results indicate that the microstructure of Mg–xLi–0.5Zn alloys can significantly influence the damping behavior of internal friction peaks and HTDB. The effect of frequency on the $\tan \delta$ value of LZ100 alloy shows that P_1 peak temperature increases with increasing frequency and its activation energy is calculated as 0.87 eV. The dependence of $\tan \delta$ value on strain amplitude in LZ100 alloy at room temperature indicates that the critical strain ε_c is 3×10^{-5} with its $\tan \delta$ value being lower than the pure Mg. The activation energy of HTDB for LZ100 is only 0.59 eV which is much lower than that of self-diffusion and grain boundary diffusion in pure Mg. This characteristic comes from the fact that the smaller atomic radius of Li atoms can diffuse more rapidly in the relatively loose BCC-structured β phase and at the abundant α/β phase boundaries which facilitates the dislocation climbing process at the same time.

Acknowledgement

The authors gratefully acknowledge the financial support of this research provided by National Science Council (NSC), Taiwan, Republic of China, under Grant NSC94-2623-7-002-005-D.

References

[1] W.F. Smith, Structure and Properties of Engineering Alloys, 2nd ed., McGraw-Hill, Singapore, 1993, p. 557.
[2] K. Sugimoto, K. Niiya, T. Okamoto, K. Kishitake, Trans. JIM 16 (1975) 647.
[3] H. Haferkamp, R. Boehm, U. Holzkamp, C. Jaschik, V. Kaese, M. Niemeyer, Mater. Trans. 42 (2001) 201.
[4] P. Metenier, G. Gonzalez-Doncel, O.A. Ruano, J. Wolfenstine, O.D. Sherby, Mater. Sci. Eng. A 125 (1990) 195.
[5] K. Higashi, J. Wolfenstine, Mater. Lett. 10 (1991) 329.
[6] M. Kawasaki, K. Kubota, K. Higashi, T. Langdon, Mater. Sci. Eng. A 429 (2006) 334.
[7] ASM Handbook, vol. 3, Alloy Phase Diagrams, ASM Int'l, Ohio, USA, 1992, pp. 2–276.
[8] K. Higashi, J. Wolfenatine, Mater. Lett. 10 (1991).
[9] I.J. Polmear, Mater. Trans. JIM 37 (1996) 12.
[10] Metals Handbook, vol. 2, 10th ed., ASM, 1990, pp. 455–479.
[11] J.Y. Wang, W.P. Hong, P.C. Hsu, C.C. Hsu, S. Lee, Mater. Sci. Forum 419–422 (2003) 165–170.
[12] T.C. Chang, J.Y. Wang, C.L. Chu, S. Lee, Mater. Lett. 60 (2006) 3272–3276.
[13] N. Saito, M. Mabuchi, M. Nakanishi, K. Kubota, K. Higashi, Scripta Mater. 36 (1997) 551.
[14] Z. Drozd, Z. Trojanova, S. Kudela, J. Alloys Compd. 378 (2004) 192.
[15] X.S. Hu, Y.K. Zhang, M.Y. Zheng, K. Wu, Scripta Mater. 52 (2005) 1141–1145.
[16] P. Barrand, Acta Metall. 14 (1966) 1247.
[17] G. Haneczok, M. Weller, Mater. Sci. Eng. A 370 (2004) 209.
[18] M. Weller, H. Clemens, G. Haneczok, Mater. Sci. Eng. A 442 (2006) 138.
[19] C.Y. Xie, E. Carreño-Morelli, R. Schaller, Scripta Mater. 39 (1998) 225.
[20] A. Vincent, J. Perez, Phil. Mag. A 40 (1979) 377.
[21] Ø. Bremnes, B. Carreño-Morelli, G. Gremaud, J. Alloys Compd. 310 (2000) 62.
[22] G. Schöck, E. Bisogni, E. Shyne, Acta Metall. 12 (1964) 1466.
[23] M. Atodiresei, G. Gremaud, R. Schaller, Mater. Sci. Eng. A 442 (2006) 160.
[24] G.A. Shirn, E.S. Wajda, H.B. Huntington, Acta Metall. 1 (1953) 513.
[25] G.A. Shirn, E.S. Wajda, H.B. Huntington, Acta Metall. 3 (1953) 409.
[26] H.J. Frost, M.F. Ashby, Deformation-Mechanism Maps, Pergamon Press, Oxford, UK, 1982.